Spatial resolution compensation by adjusting the reconstruction kernels for iterative reconstruction images of computed tomography

doi: https://doi.org/10.1016/j.ejmp.2020.05.002

Physica Medica 74 (2020) 47–55

Contents lists available at ScienceDirect

Physica Medica

journal homepage: www.elsevier.com/locate/ejmp

Technical note

Spatial resolution compensation by adjusting the reconstruction kernels for iterative reconstruction images of computed tomography

Koichi Sugisawa[a,b], Katsuhiro Ichikawa[c,*], Atsushi Urikura[d], Kazuya Minamishima[a], Shota Masuda[a], Takashi Hoshino[e], Akiko Nakahara[f], Yoshitake Yamada[g], Masahiro Jinzaki[g]

[a] Department of Radiological Technology, Keio University Hospital, 35 Shinanomachi, Shinjuku, Tokyo 160 8582, Japan
[b] Division of Health Sciences, Graduate School of Medical Science, Kanazawa University, 5-11-80 Kodatsuno, Kanazawa 920 0942, Japan
[c] Institute of Medical, Pharmaceutical and Health Sciences, Kanazawa University, 5-11-80 Kodatsuno, Kanazawa, Ishikawa 920 0942, Japan
[d] Department of Diagnostic Radiology, Shizuoka Cancer Center, 1007 Shimonagakubo, Nagaizumi, Sunto, Shizuoka 411 8777, Japan
[e] Department of Radiological Technologist, Osaka College of High Technology, 1-2-43 Miyahara, Osaka Yodogawa, Osaka 532 0003, Japan
[f] Department of Radiology, Tokyo Metropolitan Health and Medical Treatment Corporation Toshima Hospital, 33-1 Sakaecho, Itabashi, Tokyo 173 0015, Japan
[g] Department of Diagnostic Radiology, Keio University School of Medicine, 35, Shinanomachi, Shinjuku, Tokyo 160 8582, Japan

ARTICLE INFO

Keywords:
Computed tomography
Hybrid-type iterative reconstruction
Filter kernel
Spatial resolution

ABSTRACT

Purpose: Hybrid iterative reconstruction (IR) is useful to reduce noise in computed tomography (CT) images. However, it often decreases the spatial resolution. The ability of high spatial resolution kernels (harder kernels) to compensate for the decrease in the spatial resolution of hybrid IRs was investigated.

Methods: An elliptic cylindrical phantom simulating an adult abdomen was used. Two types of rod-shaped objects with ~330 and ~130 HU were inserted to simulate contrasts of arteries in CT angiography. Two multi-slice CT systems were used to scan the phantoms with 120 kVp and scan doses of 20 and 10 mGy. The task transfer functions (TTFs) were measured from the circular edges of the rod images. The noise power spectrum (NPS) was measured from the images of the water-only section. The CT images were reconstructed using a filtered back projection (FBP) with baseline kernels and two levels of hybrid IRs with harder kernels. The profiles of the clinical images across the aortic dissection flaps were measured to evaluate actual spatial resolutions.

Results: The TTF degradation of each hybrid IR was recovered by the harder kernels, whereas the noise reduction effect was retained, for both the 20 and 10 mGy. The profiles of the dissection flaps for the FBP were maintained by using the harder kernels. Even with the best combination of hybrid IR and harder kernel, the noise level at 10 mGy was not reduced to the level of FBP at 20 mGy, suggesting no capability of a 50% dose reduction while maintaining noise.

1. Introduction

Iterative reconstruction (IR) techniques have been widely used to reduce the noise in computed tomography (CT) images, and the radiation doses that facilitate the aforementioned reduction have been reported [1–5]. The IR techniques have non-linear properties with which the spatial resolution varies depending on the radiation dose (image noise) and object contrast [6]. Generally, the spatial resolution is similar to, or higher than that of the filtered back projection (FBP) under high contrast conditions, when the radiation dose is adequate. However, the resolution tends to be lower than that of the FBP under low contrast conditions when the radiation dose is low. Therefore, the task-based transfer function (TTF), which measures the spatial resolution at a specific combination of contrast and radiation dose, has been utilized to evaluate the spatial resolution of IR image [6–8]. The circular edge method is a standard procedure that is used to analyze the circular edge of the image obtained from a rod-shaped object. The attenuation (contrast) of the rod-shaped object is selected according to the clinical requirements.

The IR techniques are commonly classified into full IR and hybrid IR techniques. The full IR technique involves multiple iterations between the projection and image spaces and incorporates a more accurate model of the system. Conversely, the hybrid IR technique performs the majority of the image noise reduction in the image space in order to increase the image reconstruction speed [9]. The superiority of the full IR technique in noise reduction compared with that of the hybrid IR technique has been reported in previous studies [10–12]. However, the full IR techniques have longer reconstruction times that are unfavorable

* Corresponding author.
E-mail address: ichikawa@mhs.mp.kanazawa-u.ac.jp (K. Ichikawa).

https://doi.org/10.1016/j.ejmp.2020.05.002
Received 16 March 2020; Received in revised form 26 April 2020; Accepted 3 May 2020
Available online 11 May 2020

for routine clinical use. Thus, the hybrid IR technique is generally used, even in hospitals that possess the most advanced CT systems, while it has been reported that some hybrid IRs have limitations which include the production of images with insufficient edge preservation [6,7]. Therefore, the hybrid IRs have not demonstrated adequate noise reductions without compromising the image quality.

In this study, we investigated whether selecting reconstruction kernels with higher spatial resolutions (harder kernels) can compensate for the reduction in the spatial resolution of hybrid IRs while reducing the image noise to a level below that of FBP. TTFs of the two contrast-simulated CTA scenarios and the noise properties evaluated by a noise power spectrum (NPS) were compared between the FBP with a baseline reconstruction kernel (baseline kernel), a hybrid IR with the baseline kernel, and a hybrid IR with a harder kernel.

2. Materials and methods

2.1. Phantom

An elliptic cylindrical water phantom was used to simulate the abdomen of an adult. The phantom had outer dimensions of 300 mm × 170 mm × 190 mm, which corresponded to the width (x-direction), length (y-direction), and depth (z-direction), respectively. The two rods made of acrylic and polyoxymethylene (POM), separately, were inserted into the water phantom at offset positions 75 mm away from the center. Each rod had a diameter of 30 mm and a height of 90 mm (Fig. 1(a)). The phantom alignment of the rod was adjusted so that each rod axis was completely parallel to the rotation axis of the CT system. The POM rod (~330 HU) was used at 120 kV to simulate the CT number during the arterial phase [13,14]. The acrylic rod (~130 HU) was used to examine a severe task that simulated arteries that were insufficiently enhanced. The water-only section of the elliptic cylindrical phantom was used for the NPS measurement (Fig. 1(b)).

2.2. CT scan and reconstruction

We utilized two modern CT systems: (1) the Aquilion ONE GENESIS (CANON Medical Systems, Otawara, Japan) with a 320-row detector, and (2) the Discovery CT750 HD (GE Healthcare, Waukesha, WI) with a 64-row detector. Hereinafter, the Aquilion ONE GENESIS and CT750 HD are denoted as “Aquilion” and “CT750”, respectively. All scans were performed with 120 kVp, 0.5 s per rotation, and helical modes with pitch factors of 0.813 for Aquilion and 1.375 for CT750. Each tube current was adjusted to obtain volume CT dose indices ($CTDI_{vol}$s) of 20 and 10 mGy. The 20 mGy $CTDI_{vol}$ was selected as the standard dose, after referring to a reference value of adult abdomen to pelvis CT in the Japanese diagnostic reference levels (DRLs) [15]. The half dose (10 mGy) was used as the reduced dose condition. The detector configurations were 80 × 0.5 mm and 64 × 0.625 mm for the Aquilion and CT750, respectively. The CT images were reconstructed with a display field of view (DFOV) of 320 mm and slice thicknesses of 1.0 mm and 1.25 mm for the Aquilion and CT750, respectively. The baseline kernels were FC03 and Standard for Aquilion and CT750, respectively. The harder kernels were FC04 and FC05 for Aquilion and Detail for CT750. The hybrid IRs used for Aquilion and CT750 were adaptive iterative dose reduction three-dimensional (AIDR 3D) and adaptive statistical iterative reconstruction (ASIR), respectively. Two strengths of the AIDR 3D process (mild and strong) and two blending ratios for the ASIR (30% AISR and 100% ASIR) were selected. Table 1 summarizes these scan and reconstruction parameters.

Table 1
Scan and reconstruction parameters used in this study.

Parameters	Aquilion ONE GENESIS (Aquilion)	Discovery CT750 HD (CT750)
Reconstruction algorithms	FBP	FBP
Hybrid IR and strength	AIDR 3D, Mild and Strong	30% ASIR, and 100% ASIR
Reconstruction kernels		
Baseline kernel	FC03	Standard
Harder kernel	FC04, and FC05	Detail
Tube voltage (kVp)	120	
Volume CT dose index (mGy)	10 and 20	
Scan rotation time (sec.)	0.5	
Pitch factor	0.813	1.375
Detector configurations (mm)	80 × 0.5	64 × 0.625
Display field of view (mm)	320	
Slice thickness (mm)	1.0	1.25

2.3. TTF measurements

The TTF was measured using the previously reported circular edge method [6]. First, we applied the image averaging technique by using

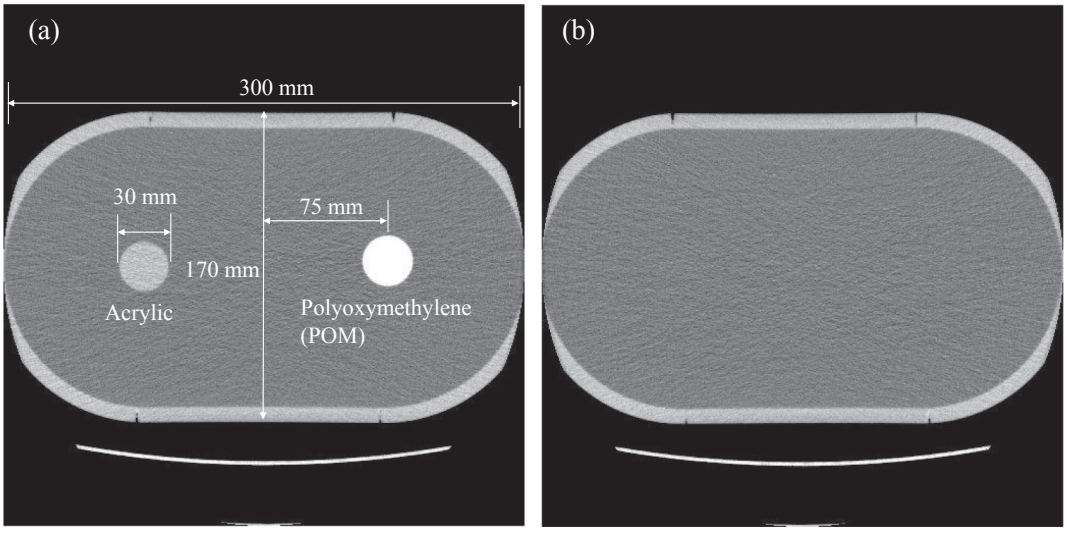

Fig. 1. Axial computed tomography (CT) images of the elliptic cylindrical water phantom including the acrylic and polyoxymethylene (POM) rods. (a) Image for task transfer function (TTF) measurement, (b) Image for noise power spectrum (NPS) measurement.

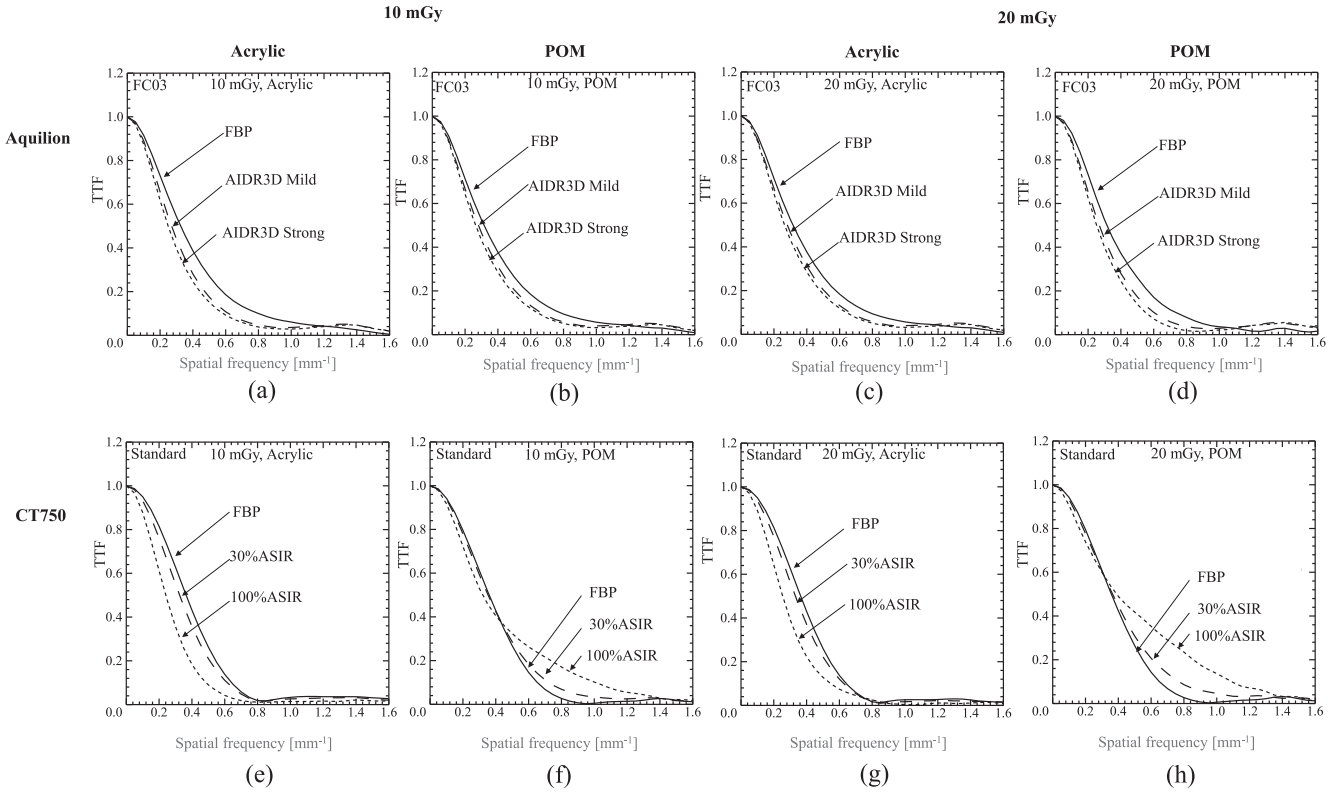

Fig. 2. TTF results of baseline reconstruction kernels (baseline kernel) at 10 and 20 mGy for the acrylic and POM contrasts. (a) – (d) Results for reconstructions of Aquilion (FBP, AIDR 3D Mild, and AIDR 3D Strong). (e) – (h) Results for reconstructions of CT 750 (FBP, 30%ASIR, and 100%ASIR).

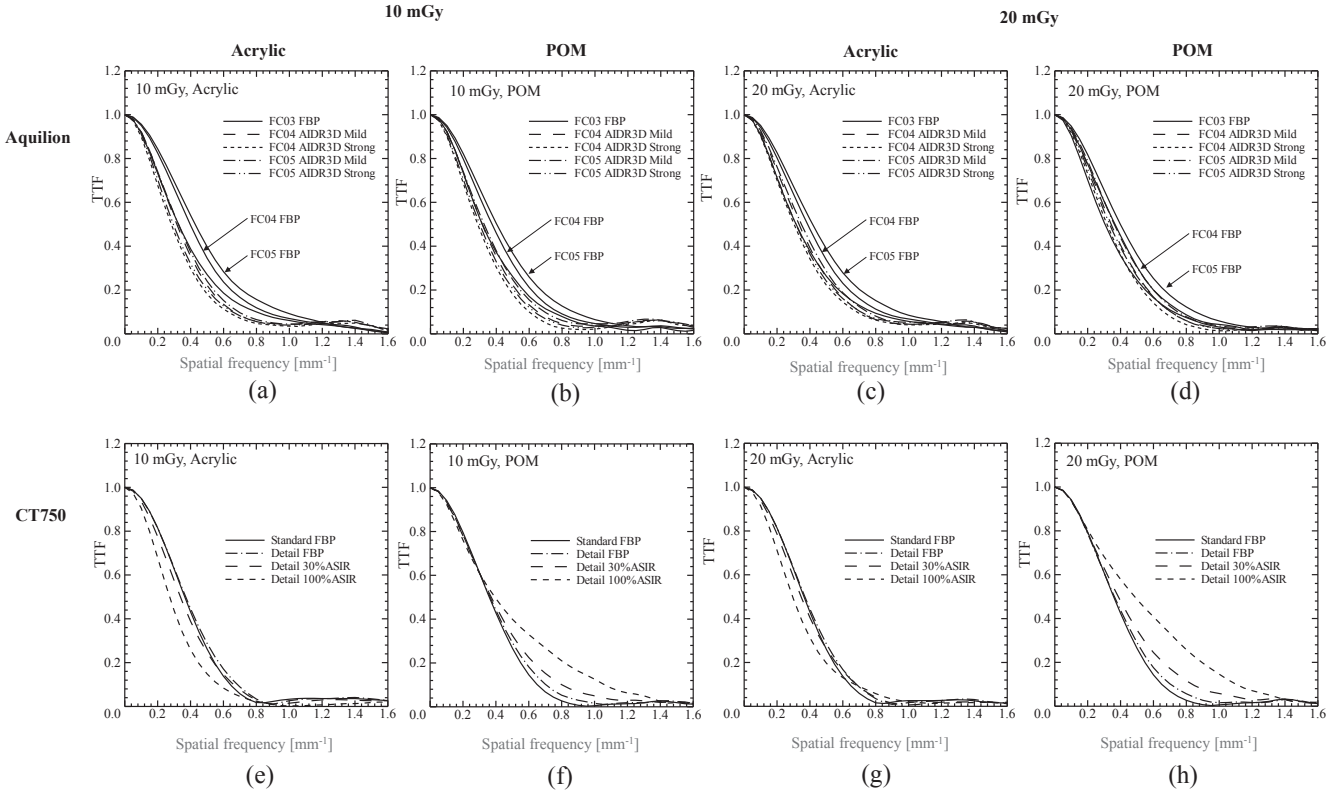

Fig. 3. TTF results of FBP with the baseline kernel and higher spatial resolution kernels (harder kernels); hybrid iterative reconstruction (IR) with harder kernels, at 10 and 20 mGy for the acrylic and POM contrasts. (a) – (d) FBP with FC03 and AIDR3D (Mild and Strong) and harder kernels (FC04 and FC05). (e) – (h) FBP with Standard and ASIR with a harder kernel of Detail.

Table 2
f_{10} and f_{50} values of the FBP and all the combinations of hybrid IRs and harder kernels. The values in parenthesis are the percent changes from each FBP with the baseline kernel at the same dose. $CTDI_{vol}$: volume CT dose index.

	$CTDI_{vol}$	Rods	f_{10} ,f_{50} TTF	Baseline kernels Reconstruction	Harder kernels Reconstruction					
Aquilion				FC03 FBP	FC04 FBP	AIDR3D Mild	AIDR3DStrong	FC05 FBP	AIDR3D Mild	AIDR3DStrong
	10 mGy	Acrylic	f_{10}	0.801	0.845 (+5.5%)	0.655 (−18.2%)	0.611 (−23.7%)	0.959 (+19.7%)	0.689 (−14.0%)	0.641 (−20.0%)
			f_{50}	0.326	0.393 (+20.6%)	0.311 (−4.6%)	0.280 (−14.1%)	0.425 (+30.4%)	0.323 (−0.9%)	0.293 (−10.1%)
		POM	f_{10}	0.727	0.770 (+5.9%)	0.646 (−11.1%)	0.594 (−18.3%)	0.860 (+18.3%)	0.690 (−5.1%)	0.628 (−13.6%)
			f_{50}	0.311	0.366 (+17.7%)	0.312 (+0.3%)	0.294 (−5.5%)	0.394 (+26.7%)	0.326 (+4.8%)	0.301 (−3.2%)
	20 mGy	Acrylic	f_{10}	0.791	0.835 (+5.6%)	0.700 (−11.5%)	0.667 (−15.7%)	0.949 (+20.0%)	0.747 (−5.6%)	0.712 (−10.0%)
			f_{50}	0.319	0.384 (+20.4%)	0.333 (+4.4%)	0.305 (−4.4%)	0.415 (+30.1%)	0.348 (+9.1%)	0.315 (−1.3%)
		POM	f_{10}	0.712	0.762 (+7.0%)	0.698 (−2.0%)	0.653 (−8.3%)	0.851 (+19.5%)	0.743 (+4.4%)	0.702 (−1.4%)
			f_{50}	0.300	0.363 (+21.0%)	0.344 (+14.7%)	0.323 (+7.7%)	0.398 (+32.7%)	0.358 (+19.3%)	0.34 (+13.3%)
CT750				Standard FBP	Detail FBP	30% ASIR	100% ASIR			
	10 mGy	Acrylic	f_{10}	0.649	0.680 (+4.8%)	0.648 (−0.2%)	0.561 (−13.6%)			
			f_{50}	0.360	0.370 (+2.8%)	0.342 (−5.0%)	0.279 (−22.5%)			
		POM	f_{10}	0.657	0.703 (+7.0%)	0.794 (+20.9%)	1.091 (+66.1%)			
			f_{50}	0.358	0.365 (+2.0%)	0.374 (+4.5%)	0.404 (+12.8%)			
	20 mGy	Acrylic	f_{10}	0.647	0.678 (+4.8%)	0.668 (+3.2%)	0.631 (−2.5%)			
			f_{50}	0.360	0.369 (+2.5%)	0.351 (−2.5%)	0.303 (−15.8%)			
		POM	f_{10}	0.654	0.699 (+6.9%)	0.830 (+26.9%)	1.121 (+71.4%)			
			f_{50}	0.357	0.363 (+1.7%)	0.388 (+8.7%)	0.488 (+36.7%)			

consecutive rod images. This technique significantly reduced the image noise, thereby facilitating accurate edge profile analyses. Contrast-to-noise ratios (CNRs) > 25 were recommended in previous studies [8,16]. As sixty to seventy consecutive axial images can be reconstructed for a single scan of the phantom, we used these images for the averaging. A one-dimensional (1D) edge spread function (ESF) was synthesized from multiple radial edges across a circular edge of the rod image. The bin width, which was used to create equidistant oversampled ESF data and to simultaneously reduce noise, was set to one-fifth of the pixel pitch corresponding to the 320-mm DFOV (0.625 mm/5 = 0.125 mm). The synthesized ESF was differentiated to yield a line spread function. The size of the dataset was then increased to 256 points by using a zero-padding technique to enable a rapid calculation of the Fourier transform. The spatial frequencies with 50% TTF and 10% TTF (f_{50} and f_{10}, respectively) were obtained from the TTF results.

2.4. NPS measurements

The NPS was measured from the uniform images of the water-only volume. An established method using the two-dimensional (2D) Fourier transform was employed [7,17,18]. One hundred images were obtained by two repeated scans of the water-only section of the phantom, and the NPS results were averaged to render the statistical error of the measurement negligible. The size of the region of interest (ROI) was set to 128 × 128 pixels at the 75-mm off-center position corresponding to the rod positions.

2.5. Edge profile and noise in clinical image

We performed profile comparisons by using clinical images of an aortic dissection. The use of clinical images was approved by our institutional review board. The comparisons were made among the FBP with a baseline kernel, the hybrid IR with a baseline kernel, and the hybrid IR with a harder kernel. One case with a typical dissection flap was selected for each the Aquilion and the CT750. An ROI with 14 × 3 ($x \times y$) pixels was used to measure the profile across a flap in a selected section (one image) of the descending aorta. CT numbers and standard deviations (SDs) were measured within the descending aorta, using ROIs with 15 × 15 pixels for five consecutive sections. The CT numbers and SDs were then respectively averaged.

3. Results

3.1. TTF measurements

The CNRs for Aquilion measured for the acrylic and POM rods were 4.6 and 11.9 at 10 mGy, respectively, while the CNRs at 20 mGy were 6.5 and 17.2, respectively. Consequently, the image numbers that are required to achieve CNRs > 25 were 30 (Acrylic) and 5 (POM) at 10 mGy and 15 (Acrylic) and 3 (POM) at 20 mGy. The image numbers for CT750 similarly estimated were almost identical with those of Aquilion. As a result, sufficient image numbers were obtained for both the 10 and 20 mGy doses to enable CNRs > 25. The reproducibility of our TTF measurements was sufficiently high as a result of the image-averaging technique; accordingly, error bars are not indicated in the TTF results because the errors were negligible.

Fig. 2 shows the results of the TTF at 10 and 20 mGy for the FBP and the hybrid IR. The AIDR 3D degraded the TTF under all conditions, whereas the ASIR degraded the TTF, especially for the acrylic object. The strong AIDR 3D process and the 100% ASIR promoted more severe TTF degradations than their mild and 30% counterparts. The TTF for the POM object was mostly preserved when the 30% ASIR was used. When 100% ASIR is used for the POM object, the TTF decreases at low frequencies but improves at middle to high frequencies. The improvements in TTF were greater with the 100% ASIR than with the 30% ASIR and were more noticeable at the 20 mGy dose.

Fig. 3 depicts the TTF results for the FBP and the hybrid IR with the harder kernels. All of the harder kernels suppressed the TTF degradations shown in Fig. 2. For 10 mGy of AIDR 3D, the TTF of the mild strength with FC05 harder kernel was nearest to that of FBP. However, the FC05 was not able to sufficiently recover the TTF to that of FBP for the acrylic object. For 20 mGy, the FC05 effectively compensated for the TTFs of the acrylic object, while the enhanced TTFs were observed for the POM object except for the strong process with the FC04 harder kernel. For the CT750 system with the acrylic object at both 10 and 20 mGy, the 30% ASIR with the Detail harder kernel provided TTFs that

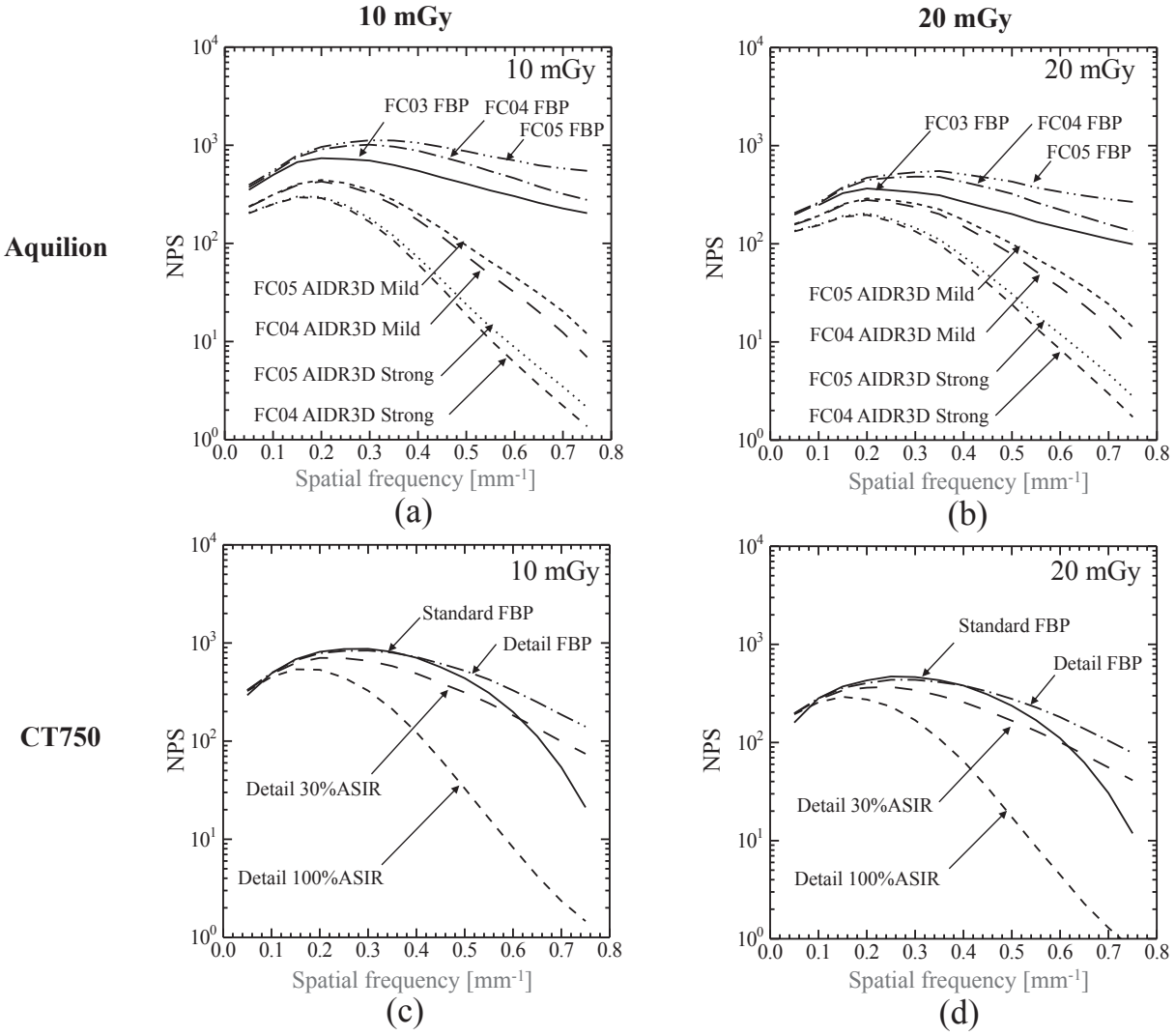

Fig. 4. Noise power spectra (NPSs) at 10 and 20 mGy for the FBP and hybrid IR with the harder kernels. (a) and (b) FBP with FC03 and AIDR 3D with the harder kernels. (c) and (d) FBP with Standard and ASIR with the harder kernel.

Table 3
Percent change of NPS for each combination of the hybrid IR and harder kernel, compared to FBP with the baseline kernel, at 0.05, 0.3, and 0.5 cycles/mm. CTDIvol: volume CT dose index.

			Harder kernels			
	$CTDI_{vol}$	Spatial frequency (cycles/mm)	Reconstruction			
Aquilion			FC04		FC05	
			AIDR3D Mild	AIDR3D Strong	AIDR3D Mild	AIDR3D Strong
	10 mGy	0.05	−33.1%	−42.3%	−32.4%	−41.3%
		0.3	−53.5%	−76.3%	−49.6%	−74.2%
		0.5	−81.6%	−95.4%	−76.5%	−94.1%
	20 mGy	0.05	−17.3%	−29.5%	−16.2%	−28.5%
		0.3	−29.3%	−60.0%	−23.2%	−56.5%
		0.5	−61.1%	−88.0%	−50.2%	−84.6%
CT750			Detail			
			30% ASIR	100% ASIR		
	10 mGy	0.05	+12.4%	+10.3%		
		0.3	−24.4%	−62.6%		
		0.5	−28.6%	−92.5%		
	20 mGy	0.05	+18.5%	+19.4%		
		0.3	−26.3%	−63.6%		
		0.5	−29.6%	−92.7%		

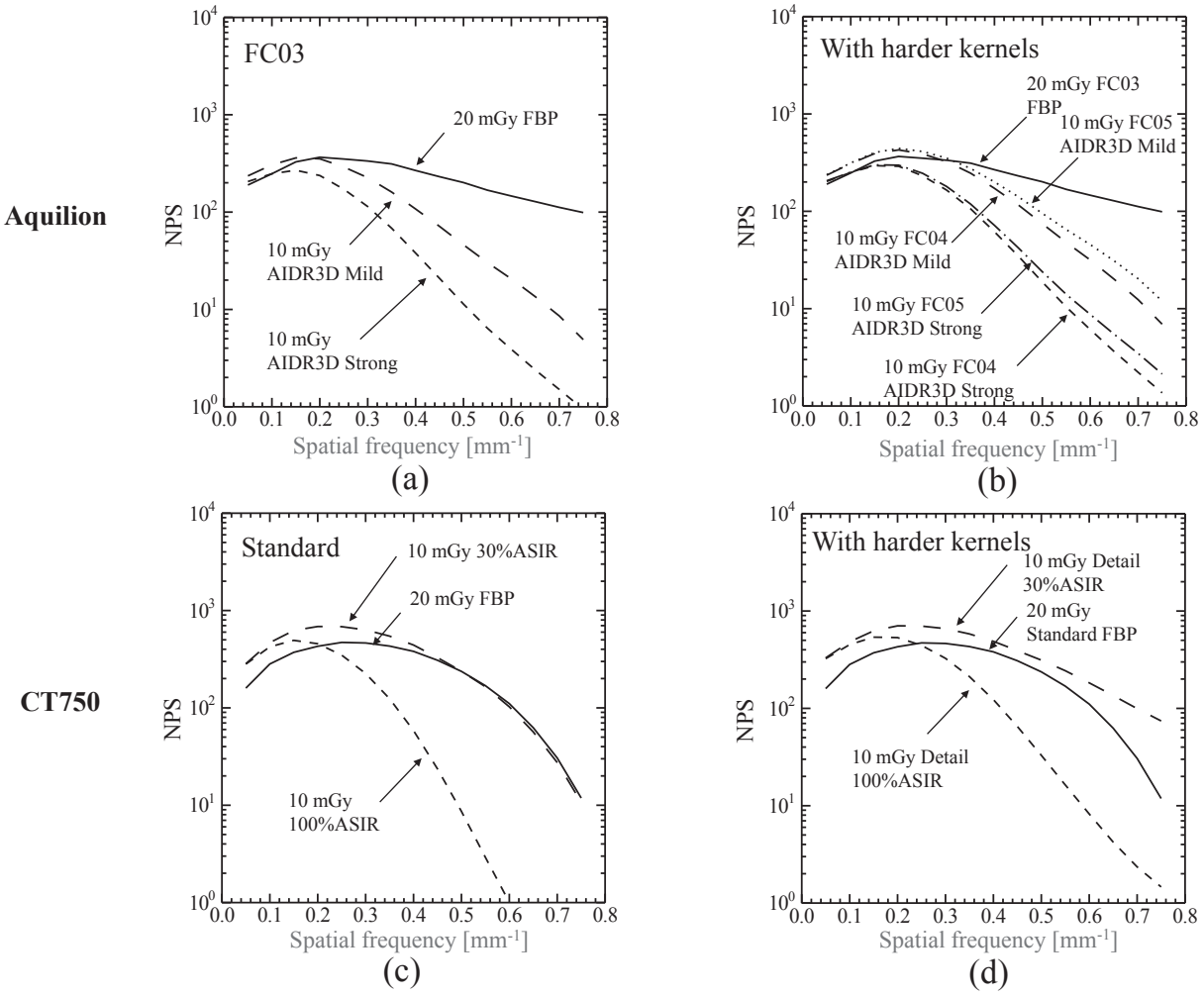

Fig. 5. NPS comparisons (a, c) between FBP at 20 mGy and hybrid IR with the baseline kernels at 10 mGy and (b, d) between FBP at 20 mGy and hybrid IR with harder kernels at 10 mGy.

reasonably approximated those of the FBP. Enhanced TTFs were observed at both 10 and 20 mGy for the POM object. Table 2 shows the f_{10} and f_{50} values calculated from the TTF curves of the FBP and all the combinations of the hybrid IR and harder kernel. The percent changes based on f_{10} and f_{50} of FBP with the baseline kernel are also presented.

3.2. NPS measurements

Fig. 4 shows the NPS results of the FBP and hybrid IRs with the harder kernels. Because one hundred images were used to average many NPS results for each reconstruction, the error of NPS evaluation was negligible. Table 3 shows the percent change of NPS for each combination of the hybrid IR and harder kernel, compared to FBP with the baseline kernel, at 0.05, 0.3, and 0.5 cycles/mm. Most of the proposed conditions reduced the NPSs compared with the FBP. The reductions were more notable with higher strengths (blending rates) of the hybrid IRs. The AIDR 3D decreased the NPSs over the entire spatial frequency range. The degree of noise reduction was more notable at high spatial frequencies than at low to middle frequencies. On the other hand, the ASIR presented the NPS changes like low-pass filtering, which depicted nearly unchanged NPS values at the lowest frequency and an NPS decrease with the increase in spatial frequency. Fig. 5 shows the NPSs of the FBP at 20 mGy and the hybrid IR at 10 mGy. The NPS of the strong AIDR 3D at 10 mGy is almost lower than that of the FBP at 20 mGy, whereas the mild process exhibits higher NPSs compared with that of the FBP at low frequencies. The ASIR could not reduce the noise at 10 mGy to the level achieved by that of FBP at 20 mGy. Although lower NPSs were observed at frequencies $>$ 0.25 cycles/mm for the 100%ASIR, the noise level at low frequencies was notably higher than that of FBP at 20 mGy.

3.3. Appropriate combinations

We proposed an appropriate combination of hybrid IR strength and harder kernel that provide the following: (1) TTF that is similar to that of the FBP for the acrylic object and (2) NPS that is lower than that of the FBP. As a result, the mild process with FC05 for the Aquilion system and the 30% ASIR with Detail for the CT750 system were selected. With these combinations, enhanced TTFs are obtained for the POM object (330 HU) at 20 mGy for the Aquilion system and at 10 and 20 mGy for the CT750 system.

3.4. Rod images

Fig. 6 shows the rod images for the FBP with the baseline kernel and the hybrid IR with harder kernels. We were able to observe the states of edge preservation and noise reduction, corresponding to the TTF and NPS results, respectively, in which both the mild process with the FC05 harder kernel and the 30% ASIR with the Detail harder kernel presented edge preservations and noise reductions compared with those of the FBP. Sharper edges (edge enhancement) were observed in the images with 100% ASIR when compared with that of the FBP for the POM

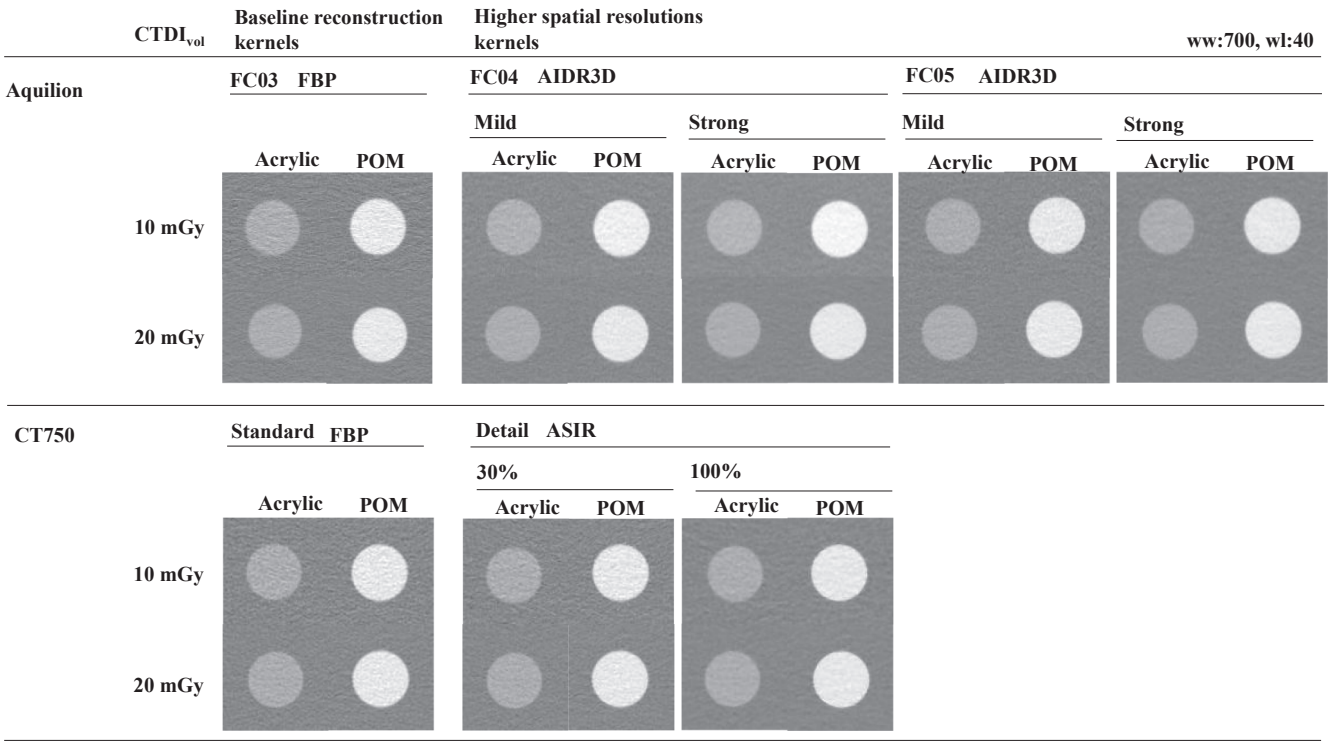

Fig. 6. Images of acrylic and POM rods at 10 and 20 mGy, for FBP with the baseline kernel and combinations of hybrid IR and the harder kernel.

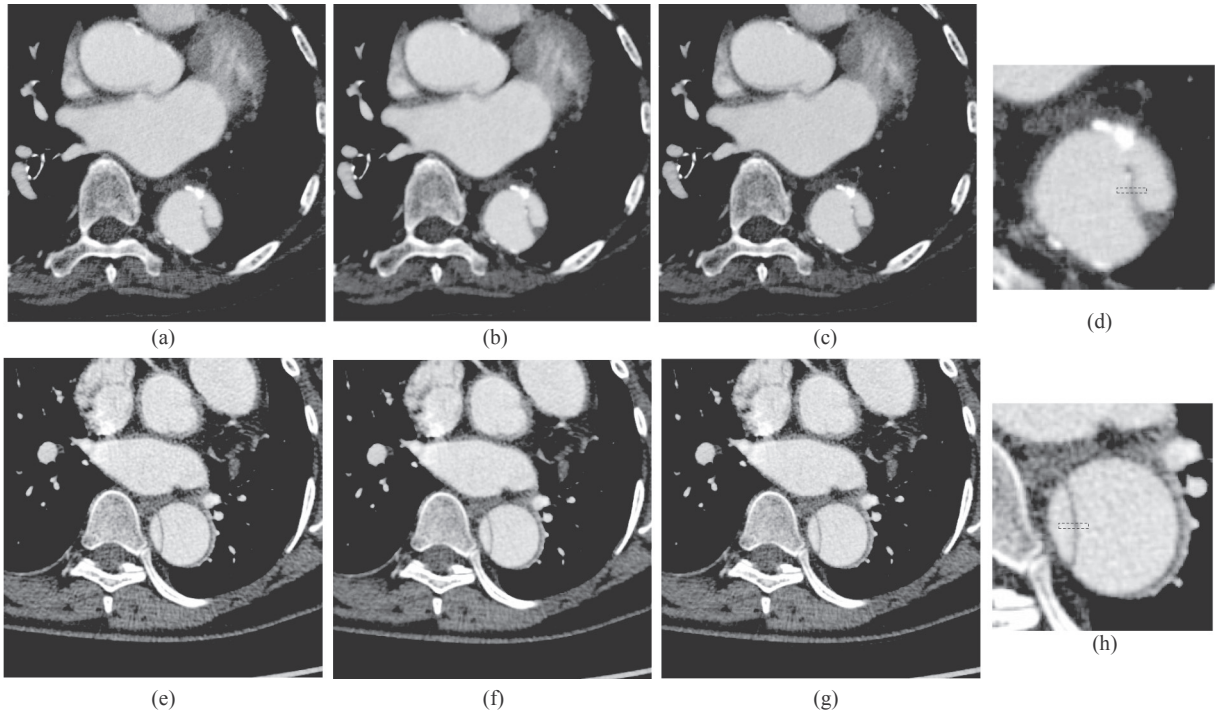

Fig. 7. Comparisons of clinical images with aortic dissections for (a) – (c) FBP with FC03, Mild with FC03, and Mild with FC05; (e) – (g) FBP with Standard, 30% ASIR with Standard, and 30% ASIR with Detail. The volume computed tomography dose index ($CTDI_{vol}$) for Aquilion and CT750 cases were 10.0 and 10.1 mGy, respectively. ROI positions for profile measurements across the dissection flap are also indicated in magnified images of descending aorta (d, h).

object.

3.5. Image noise and profile across dissection flap

Fig. 7 shows the clinical images with aortic dissections obtained using the Aquilion and CT750. The acquisition parameters were: 120 kVp, 0.5 s per rotation, and pitch factors of 0.813 (for Aquilion) and 1.375 (for CT750). The tube currents were adjusted by the tube current modulation systems of each system. The setting values were: SD = 10.5 for the Volume Exposure Control (Volume EC) of Aquilion and noise index = 13.5 for the CT Automatic Exposure Control (CT AEC) of CT750. The reported $CTDI_{vol}$ of Aquilion and CT750 were 10.0 and

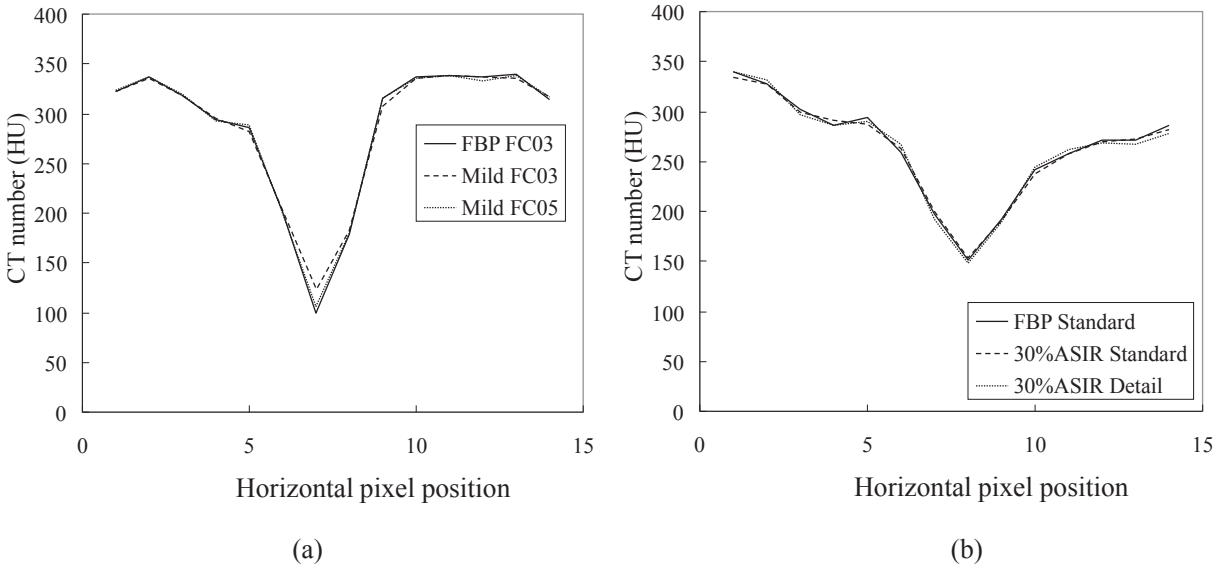

Fig. 8. Comparisons of profiles across the dissection flaps (shown in Fig. 7) between FBP with the baseline kernel, hybrid IR with the baseline kernel, and the appropriate combination of hybrid IR and harder kernel. (a) Aquillion, (b) CT750.

10.1 mGy, respectively. The CT numbers were 301.1, 300.9, and 300.0 HU for the FBP with FC03, mild process with FC03, and mild process with FC05, respectively, while the corresponding SD values were 20.0, 14.9, and 18.2 HU. On the other hand, the CT numbers were 324.7, 324.6, and 324.5 HU for the FBP with Standard, 30% ASIR with Standard, and 30% ASIR with Detail, respectively. The corresponding SD values were 33.1, 27.5, and 30.3 HU. Since the CT numbers were sufficiently high, these cases were considered to follow the results of the POM object. Fig. 8 shows the comparisons of the profiles across the dissection flaps. For Aquilion, even though the image of the mild process with FC03 (the baseline kernel) revealed less noise, the dissection flaps were blurred compared with the FBP. The CT number at the flap was increased by 20.5%. In contrast, the mild process with FC05 (the harder kernel) exhibits edge preservations and lower noises compared with FBP. The low CT number at the flap in the profile of Aquilion's FBP was adequately reproduced by the mild process with FC05, presenting a slight CT number increase of 3.5%, which demonstrated that the harder kernels were capable of recovering the spatial resolution. On the other hand, for CT750, the CT numbers at the flap were almost identical between FBP with Standard, 30% ASIR with Standard, and 30% ASIR with Detail, corresponding to the well-preserved TTF of the POM object for 30% ASiR.

4. Discussion

In the present study, we evaluated the task-based spatial resolution and image noise for the FBP and various combinations of hybrid IR strengths and harder kernels. We also defined the 330-HU contrast of POM and the 130-HU contrast of acrylic as tasks corresponding to the enhanced and insufficiently enhanced arteries, respectively.

The AIDR 3D degraded the TTFs for both the acrylic and POM objects. Therefore, in the absence of the harder kernels, image blurring of enhanced arteries is unavoidable. The ASIR showed TTFs with a contrast dependency. The TTFs were degraded for the acrylic object but enhanced for the POM object. Consequently, the ASIR could still be used without the harder kernels, once the arteries are sufficiently enhanced. It can be considered that the 130-HU contrast (acrylic object) approximates contrasts at soft-tissue organ edges surrounded by abdominal fats because of the attenuations of 50–60 HU for the soft-tissues and −100 HU for the fat. Thus, our TTF results suggest that the soft-tissue organ edges are somewhat blurred in images of both AIDR 3D and ASIR with the baseline kernels. In this case, the harder kernel would also be effective in recovering the sharpness of the organ edges.

Our measurements and rod images demonstrated that the TTF reductions caused by the hybrid IRs for the baseline kernels were mostly recovered by the combination of mild strengths with FC05 harder kernels and 30% ASIR with Detail harder kernels. The noise reductions by the hybrid IRs were maintained, even with these combinations, while the 30%ASIR with Detail showed modest noise increases compared with that of the FBP in high spatial frequencies > 0.6 cycles/mm. Thus, the combinations of hybrid IR and harder kernel we selected were suggestive as useful ones for noise reduction of abdominal CTA images.

The clinical images of aortic dissection flap showed states of the spatial resolution and noise corresponding to the results of the phantom study for the POM object simulating a contrast in artery phase. Since the mild strengths degraded the TTF with FC03 for Aquilion, the CT number at dissection flap accordingly rose. This rise was compensated by the harder kernel FC05, while the noise remained lower than that of FBP. On the other hand, corresponding to the TTF result for the POM object not degraded by 30% ASiR, the CT number at the dissection flap was not mostly affected.

The 50% dose reduction capabilities were analyzed by TTF preservations and NPS reductions, comparing the FBP at 20 mGy with the hybrid IR at 10 mGy (Fig. 5). Both the AIDR 3D and the ASIR were unable to achieve the 50% dose reduction for the conditions we tested in this study. Although the strong AIDR 3D largely recovered the noise at 10 mGy to the same level of that of FBP at 20 mGy, this combination did not preserve the TTF of the FBP. The ASIR was not able to reduce the low frequency noise, even with 100% blending. When a half dose is used with ASIR, the visibilities of low contrast objects such as hypovascular tumors might be impaired by the increased low frequency noise. These properties are also observed in the rod images in Fig. 6. In comparison with the same dose, both the mild process with FC05 and the 30% ASIR with Detail exhibited lower noise and mostly preserved the edge sharpness compared with that of FBP. However, their observed noise levels at 10 mGy were higher than those of FBP at 20 mGy. Also, there was a decrease in the noise level for the strong process with FC05 at 10 mGy compared with that of the FBP at 20 mGy. However, there was insufficient edge preservation, particularly for the acrylic object.

These implications have been discussed within the community of Japanese radiological technologists with PhDs and clinical experience in CTA. However, the quantitative evaluations using the harder kernels have not been published in any papers. The hybrid IRs are still used in many hospitals because the model-based iterative reconstruction

techniques are rarely installed due to their high cost and prolonged reconstruction times. Thus, our findings have significant implications for facilities that are still routinely using hybrid IRs.

The present study possesses several limitations. First, we only measured the TTFs from 30-mm diameter rods. Thus, it is possible that the spatial resolution in complex shapes might not be correctly evaluated. Although no shape dependencies of the TTF were reported in a previous study [8], evaluations using phantoms of various shapes are required. Second, only two CT systems were investigated in this study. Thus, the effectiveness of the combination of hybrid IRs and harder kernels might not be applicable to other CT systems. Third, only one phantom size resembling a Japanese adult abdomen was investigated; thus, the effects on thick patients should be examined using phantoms with bigger sizes. Forth, we used a tube voltage of 120 kV. Lower tube voltages recently used in CTA should be evaluated. Finally, we did not perform a human observer study using clinical abdominal CTA images. Consequently, further studies to validate our findings in clinical images are required.

5. Conclusion

This study evaluated the task-based spatial resolution and image noise for CT acquisition conditions corresponding to abdominal CTAs. Various combinations of hybrid IR strengths and harder kernels were used to investigate whether the use of harder kernels compensates for the degradation of spatial resolution of the hybrid IR while maintaining the ability to reduce noise. Our findings indicated that the use of harder kernels was effective for recovering the TTF that was degraded by hybrid IRs, with the maintenance of the noise reductions. The 50%-dose reduction capabilities without TTF degradations were not indicated for hybrid IRs we tested.

Declaration of Competing Interest

The authors declare that they have no known competing financial interests or personal relationships that could have appeared to influence the work reported in this paper.

Acknowledgements

The authors thank Takuya Yokota and Yosuke Kogure at Department of radiology, Juntendo university hospital, Keisuke Kizu, Ryo Tsukada, and Akihisa Yamazaki at Department of radiological technology, Keio university hospital, for their valuable technical assistance.

References

[1] Miéville FA, Gudinchet F, Brunelle F, Bochud FO, Verdun FR. Iterative reconstruction methods in two different MDCT scanners: Physical metrics and 4-alternative forced-choice detectability experiments – a phantom approach. Phys Medica 2013;29:99–110. https://doi.org/10.1016/j.ejmp.2011.12.004.
[2] Berta L, Mascaro L, Feroldi P, Maroldi R. Optimisation of an MDCT abdominal protocol: image quality assessment of standard vs. iterative reconstructions. Phys Medica 2014;30:271–9. https://doi.org/10.1016/j.ejmp.2013.07.126.
[3] Aurumskjöld ML, Ydström K, Tingberg A, Söderberg M. Improvements to image quality using hybrid and model-based iterative reconstructions: a phantom study. Acta Radiol 2017;58:53–61. https://doi.org/10.1177/0284185116631180.
[4] Yamada Y, Jinzaki M, Hosokawa T, Tanami Y, Sugiura H, Abe T, et al. Dose reduction in chest CT: Comparison of the adaptive iterative dose reduction 3D, adaptive iterative dose reduction, and filtered back projection reconstruction techniques. Eur J Radiol 2012;81:4185–95. https://doi.org/10.1016/j.ejrad.2012.07.013.
[5] Greffier J, Pereira F, Macri F, Beregi JP, Larbi A. CT dose reduction using Automatic Exposure Control and iterative reconstruction: a chest paediatric phantoms study. Phys Medica 2016;32:582–9. https://doi.org/10.1016/j.ejmp.2016.03.007.
[6] Richard S, Husarik DB, Yadava G, Murphy SN, Samei E. Towards task-based assessment of CT performance: System and object MTF across different reconstruction algorithms. Med Phys 2012;39:4115–22. https://doi.org/10.1118/1.4725171.
[7] Samei E, Richard S. Assessment of the dose reduction potential of a model-based iterative reconstruction algorithm using a task-based performance metrology. Med. Phys 2015;42:314–23.
[8] Takata T, Ichikawa K, Mitsui W, Hayashi H, Minehiro K, Sakuta K, et al. Object shape dependency of in-plane resolution for iterative reconstruction of computed tomography. Phys Med 2017;33:146–51.
[9] Ehman EC, Yu L, Manduca A, Hara AK, Shiung M, Jondal D, et al. Methods for clinical evaluation of noise reduction techniques in abdominopelvic CT. Radiographics 2014;34:849–62.
[10] Yamada Y, Jinzaki M, Niijima Y, Hoshimoto M, Yamada M, Abe T, et al. CT Dose Reduction for Visceral Adipose Tissue Measurement: Effects of Model-Based and Adaptive Statistical Iterative Reconstructions and Filtered Back Projection Methods for clinical evaluation of noise reduction techniques in abdominopelvic CT. Radiographics 2014;34:849–62.
[11] Yasaka K, Furuta T, Kubo T, Maeda E, Katsuta T, Sato J, et al. Full and hybrid iterative reconstruction to reduce artifacts in abdominal CT for patients scanned without arm elevation. Acta Radiol 2017;58:1085–93.
[12] Laurent G, Villani N, Hossu G, Rauch1 A, Noël A, Blum1 A, et al., Full model-based iterative reconstruction (MBIR) in abdominal CT increases objective image quality, but decreases subjective acceptance, European Radiology. 2019;29:4016–25.
[13] Hoshika M, Yasui K, Niguma T, Kojima T, Nishiyama N, Suzuki D, et al. Novel contrast-injection protocol for high-resolution abdominal CT-angiography: vascular visualization improvement with vasodilator. Abdom Radiol 2017;42:2571–8.
[14] Altenbernd J, Wetter A, Forsting M, Umutlu L. Dual-energy CT of liver metastases in patients with uveal melanoma. Eur J Radiol Open 2016;3:254–8.
[15] Japan Network for Research and Information on Medical Exposure (J-RIME), Diagnostic Reference Levels Based on Latest Surveys in Japan (Japan DRLs 2015). http://www.radher.jp/J-RIME/report/DRLhoukokusyoEng.pdf.
[16] Urikura A, Ichikawa K, Nishimaru E, Nakaya Y. Spatial resolution measurement for iterative reconstruction by use of image-averaging techniques in computed tomography. Radiol Phys Technol 2014;7:358–66.
[17] Kawashima H, Ichikawa K, Matsubara K, Nagata H, Akata T, Kobayashi S. Quality evaluation of image-based iterative reconstruction for CT: comparison with hybrid iterative reconstruction. J Appl Clin Med Phys 2019;20(6):199–205. https://doi.org/10.1002/acm2.12597.
[18] Urikura A, Hara T, Ichikawa K, Nishimaru H, Hoshino T, Yoshida T, et al. Objective assessment of low-contrast computed tomography images with iterative reconstruction. Phys Med 2016;32:992–8.